SUPPLEMENTARY INFORMATION

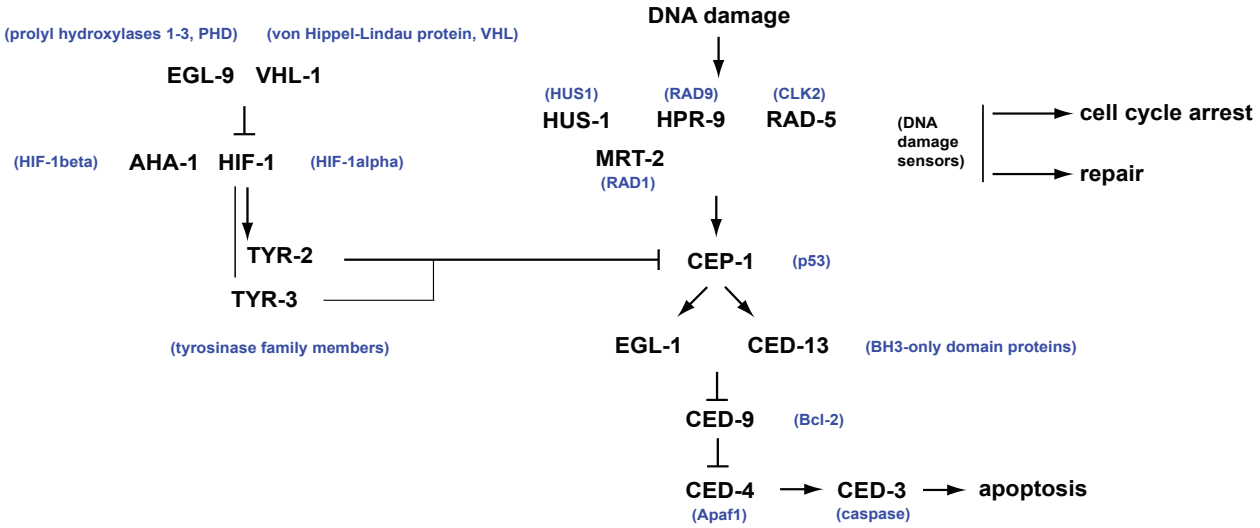

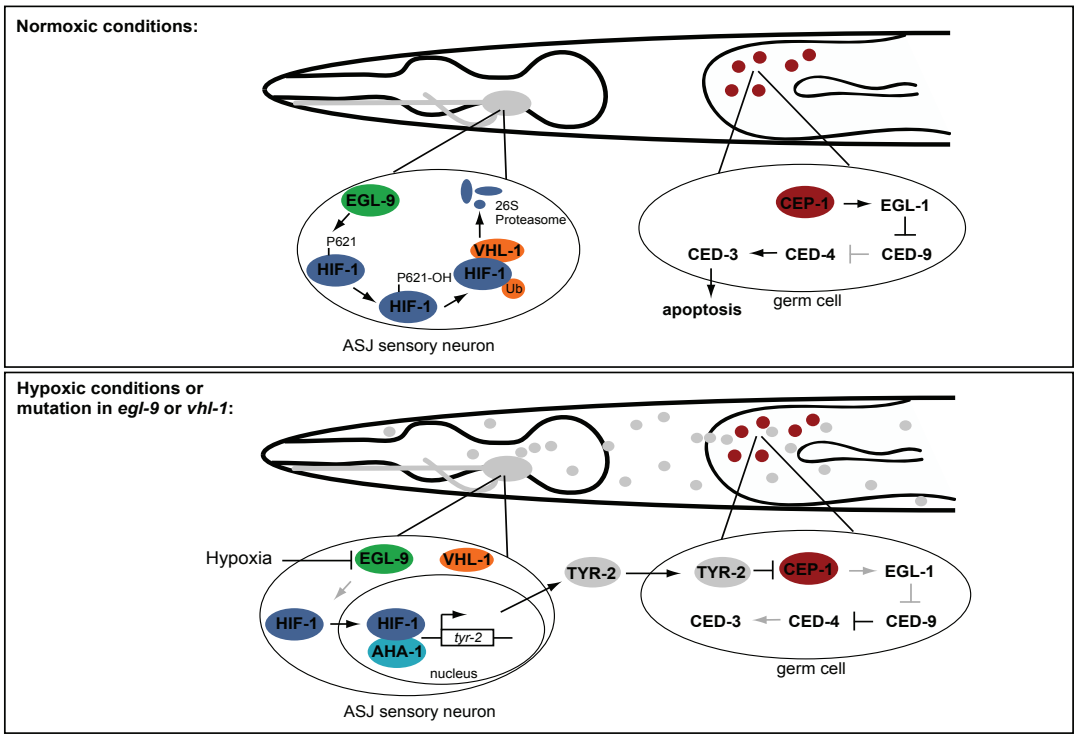

Supplementary Figure 1. Summary of the pathway by which HIF-1 antagonizes IR-induced apoptosis in *C. elegans*. In *C. elegans,* DNA damage is recognized by a conserved sensor pathway consisting of members of the 9-1-1 complex (HUS-1, MRT-2 and HPR-9) and RAD-5 that acts in parallel to the 9-1-1 complex [39, 47]. This sensor pathway is necessary for the induction of apoptosis, cell cycle arrest and repair initiation. In contrast, the p53 homolog CEP-1 mediates only the apoptotic response upon DNA damage, but is dispensable for cell cycle arrest and repair. CEP-1/p53 transcriptionally regulates the BH3-only domain proteins EGL-1 and CED-13, which initiate apoptosis via the core apoptotic machinery consisting of CED-9, CED-4 and CED-3 (ref. 11, 12). *vhl-1(ok161)* mutant animals are resistant to DNA damage-induced apoptosis due to stabilized HIF-1 in the two ASJ sensory neurons which are part of the chemosensory organ of the animal. This antiapoptotic effect is mediated to a large part via transcriptional upregulation and secretion of TYR-2. TYR-2 acts genetically as negative regulators of CEP-1/p53, thereby inhibiting apoptosis following DNA damage. *C. elegans* proteins are in black, mammalian counterparts in blue.

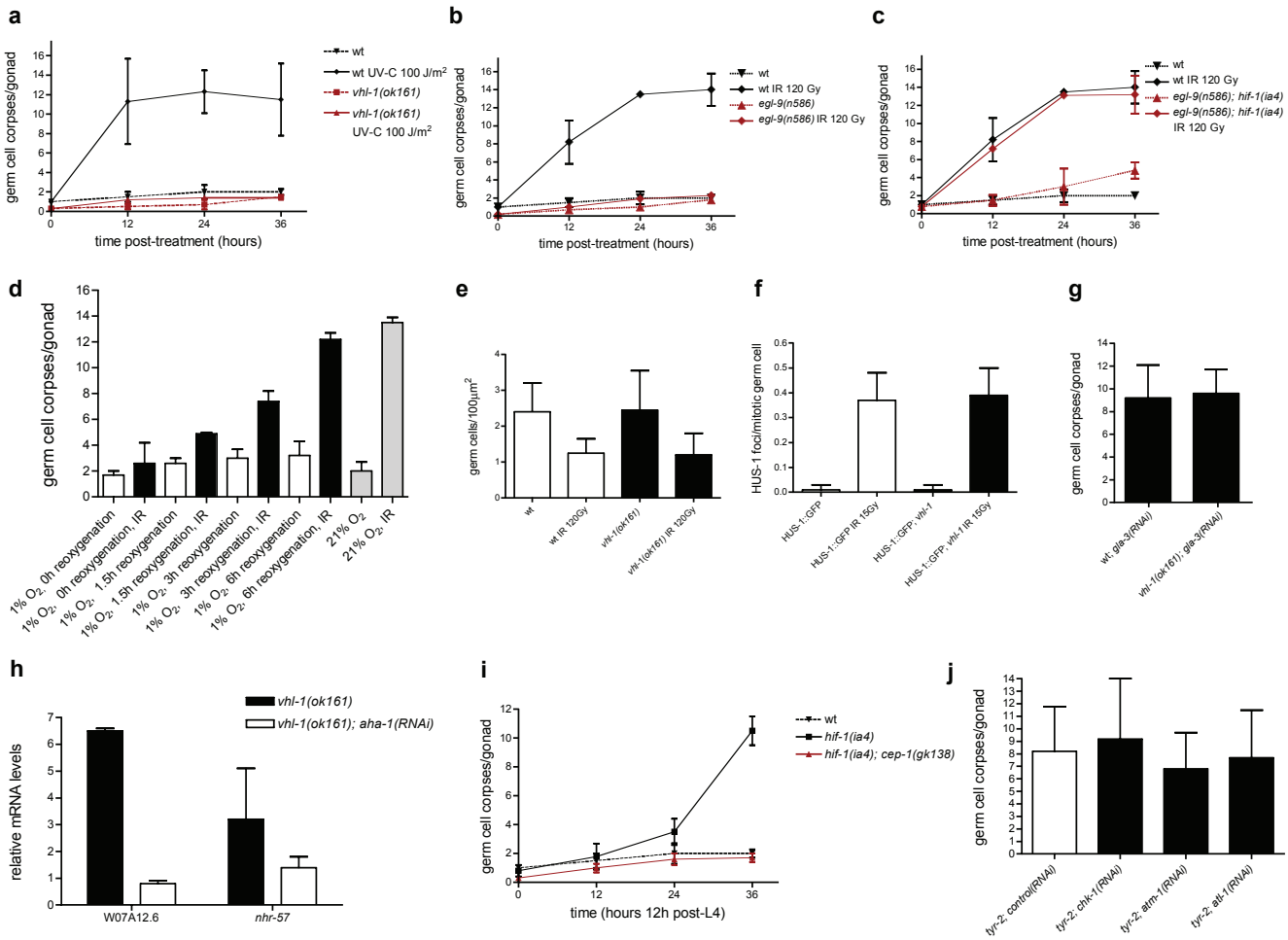

Supplementary Figure 2. HIF-1 upregulation via hypoxia treatment or loss of *egl-9* function confers resistance to IR.
a, HIF-1 antagonizes apoptosis following UV-C exposure. Synchronized young adult worms were exposed to 100 J/m2 UV-C and germline apoptosis was quantified at the indicated time points. Data shown represent the average of 40 worms per time point ± s.d.
b-c, Quantification of germline apoptosis. Synchronized young adult hermaphrodites were exposed to IR and germline apoptosis was quantified at the indicated time points. Data shown represent the average of three to six independent experiments ± s.d. (n>20 animals for each experiment and time point).
d, Synchronized young adult wild-type animals were irradiated and subsequently transferred to the hypoxia chamber for 24 hours at 1% oxygen, 23°C. Germline apoptosis of irradiated and control animals was quantified immediately after the end of the hypoxia treatment, and at the indicated time points. Data shown represent the average of 50 worms per time point ± s.d.
e, Cell cycle arrest is not affected by HIF-1. Synchronized young adults were irradiated and the number of cells in the mitotic zone was assessed 12 hours post-treatment. Data shown represent the average of three independent experiments ± s.d. (n>15 per experiment)
f, HUS-1 localizes to distinct foci irrespective of HIF-1. Synchronized wild-type or *vhl-1(ok161)* animals bearing the HUS-1::GFP reporter were irradiated with 15 Gy. Gonads were dissected and assessed for appearance of HUS-1 foci in the mitotic germline zone three hours post-treatment. Data shown represent the average of 10 analyzed gonads ± s.d.
g, *gla-3(RNAi)* results as *ced-9(RNAi)* in increased levels of germ cell apoptosis in *vhl-1(ok161)* mutants.
Germline apoptosis quantification 36 hours post-L4 stage in synchronized wild-type or *vhl-1(ok161)* animals fed on *gla-3(RNAi)*.
Data shown represent the average of 40 worms per time point ± s.d.
h, Knock-down of the worm HIF-1beta homolog *aha-1* efficiently inhibits transcriptional upregulation of HIF-1 target genes.
Synchronized L3 stage larvae were transferred to *aha-1(RNAi)* expressing bacteria, and mRNA levels of two HIF-1 target genes (W07A12.6 and *nhr-57*) were measured by qRT-PCR as young adults. mRNA levels are relative to wild-type mRNA levels from three independent experiments ± s.d.
i, Increased basal level of apoptosis in *hif-1(ia4)* mutants is dependent on CEP-1/p53 function. Germ cell apoptosis quantification of unirradiated young adult animals. Data shown represent the average of three independent experiments ± s.d. (n>20 per time point and experiment).
j, Germ cell apoptosis quantification 36 hours post-L4 stage in synchronized animals. Data shown represent the average 34-40 animals ± s.d.

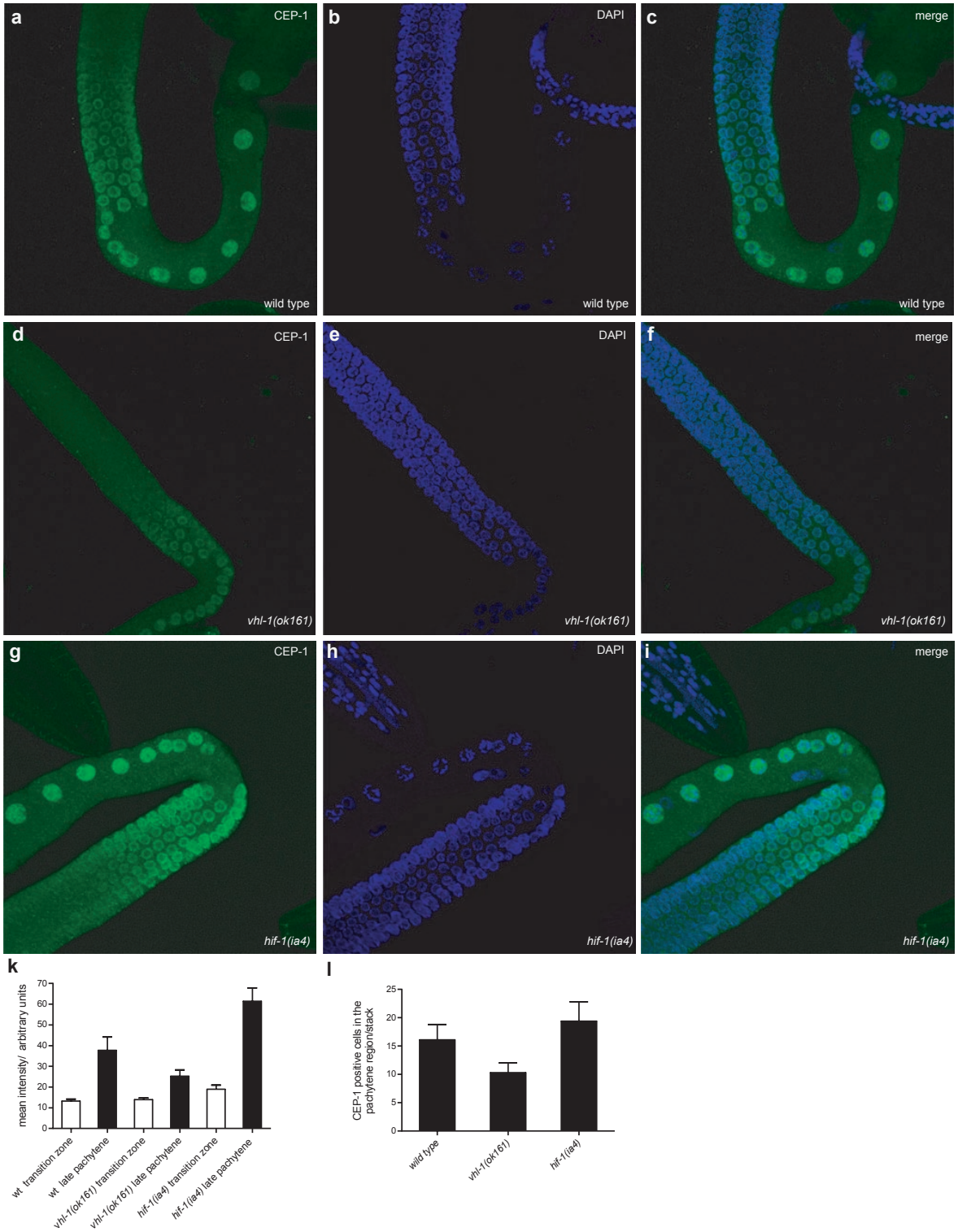

Supplementary Figure 3 CEP-1 levels in the pachytene region of the germ line are negatively regulated by HIF-1.
a-i, Wild-type, *vhl-1(ok161)* and *hif-1(ia4)* dissected gonads were fixed at 12h post-L4 stage and incubated with anti-CEP-1 antibody and DAPI.
k, Quantification of the mean intensity of CEP-1 in late pachtytene germ cells compared to the background levels of the transition zone in wild-type, *vhl-1(ok161)* and *hif-1(ia4)* animals using ImageJ. Data shown represent the average cell intensity of 15 stacks ± s.d.
l, Quantification of the number of CEP-1 positive pachytene germ cells in wild-type, *vhl-1(ok161)* and *hif-1(ia4)* animals. Data shown represent the average of 17-19 stacks ± s.d.

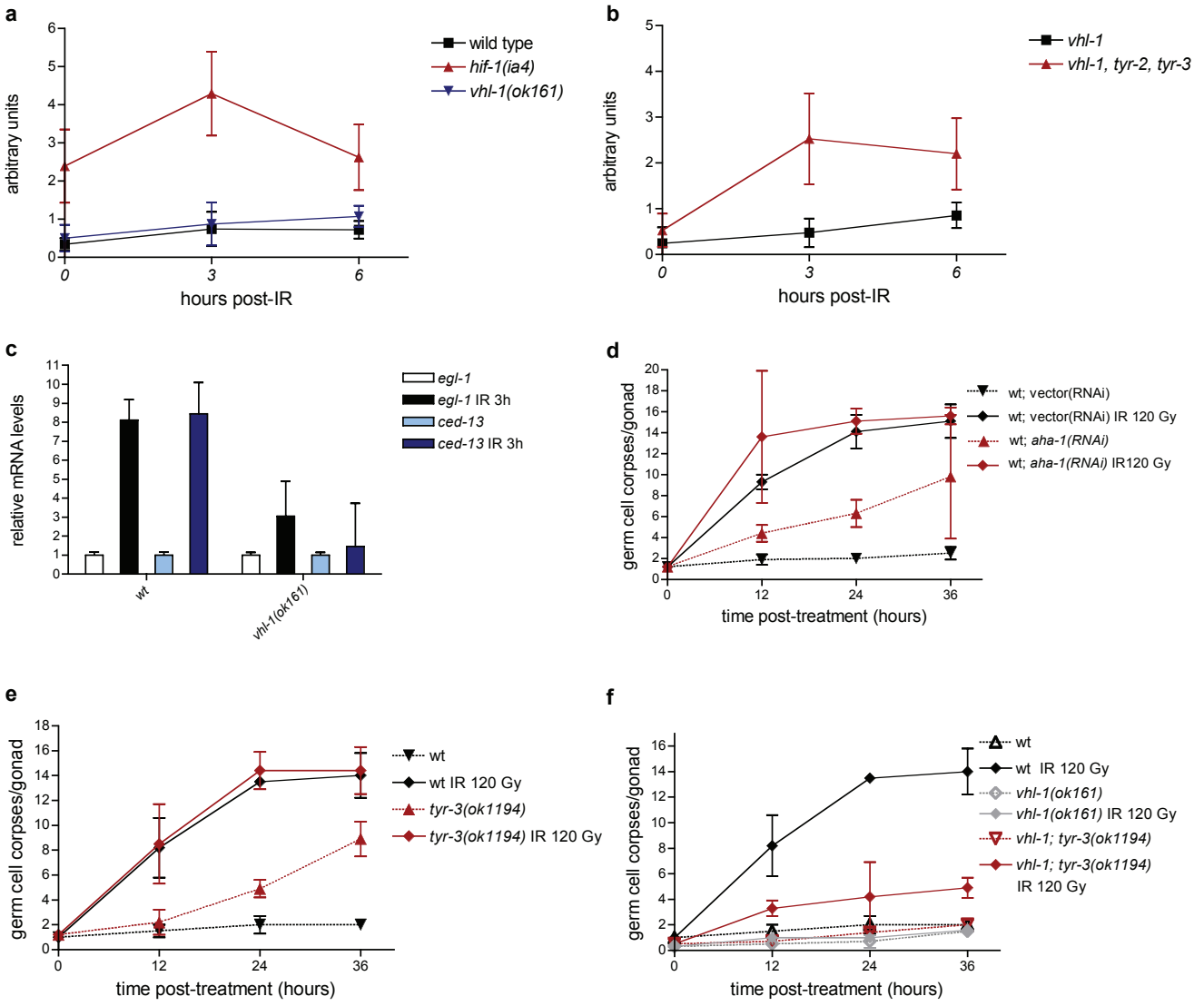

Supplementary Figure 4. Quantification of CEP-1/p53 western blots and CEP-1/p53 function.
a, Quantification of CEP-1/p53 western blots (total protein) in wild-type, *hif-1(ia4)* and *vhl-1(ok161)* animals following IR 120 Gy using ImageJ. Data shown represent the average of three western blots ± s.d.
b, Quantification of CEP-1/p53 western blots (total protein) in *vhl-1* and *vhl-1; tyr-2; tyr-3* mutant animals following IR 120 Gy using ImageJ. Data shown represent the average of three western blots ± s.d.
c, CEP-1/p53 target gene induction is decreased in *vhl-1(ok161)* mutant animals.
As a readout for CEP-1/p53 function, induction of two CEP-1/p53 target genes were assessed. Synchronized young adult wild-type and *vhl-1(ok161)* animals were analyzed for *egl-1* and *ced-13* mRNA levels following IR 120 Gy by quantitative RT-PCR. Transcript levels were normalized to *tbp-1* and *pgk-1*. Data shown represents the average of four independent experiments ± s.d.
d, Wild-type animals were grown on bacteria containing either an empty control RNAi vector or the HIF-1beta homolog *aha-1(RNAi)* beginning at the third larval stage (L3). Synchronized young adult animals were irradiated and germline apoptosis was quantified at the indicated time points. Data shown represent the average of three independent experiments ± s.d. (n>20 per time point and experiment).
e-f, Time course analysis of germ cell apoptosis in synchronized control or irradiated young adult animals. Data shown represent the average of three to six independent experiments ± s.d. (n>20).

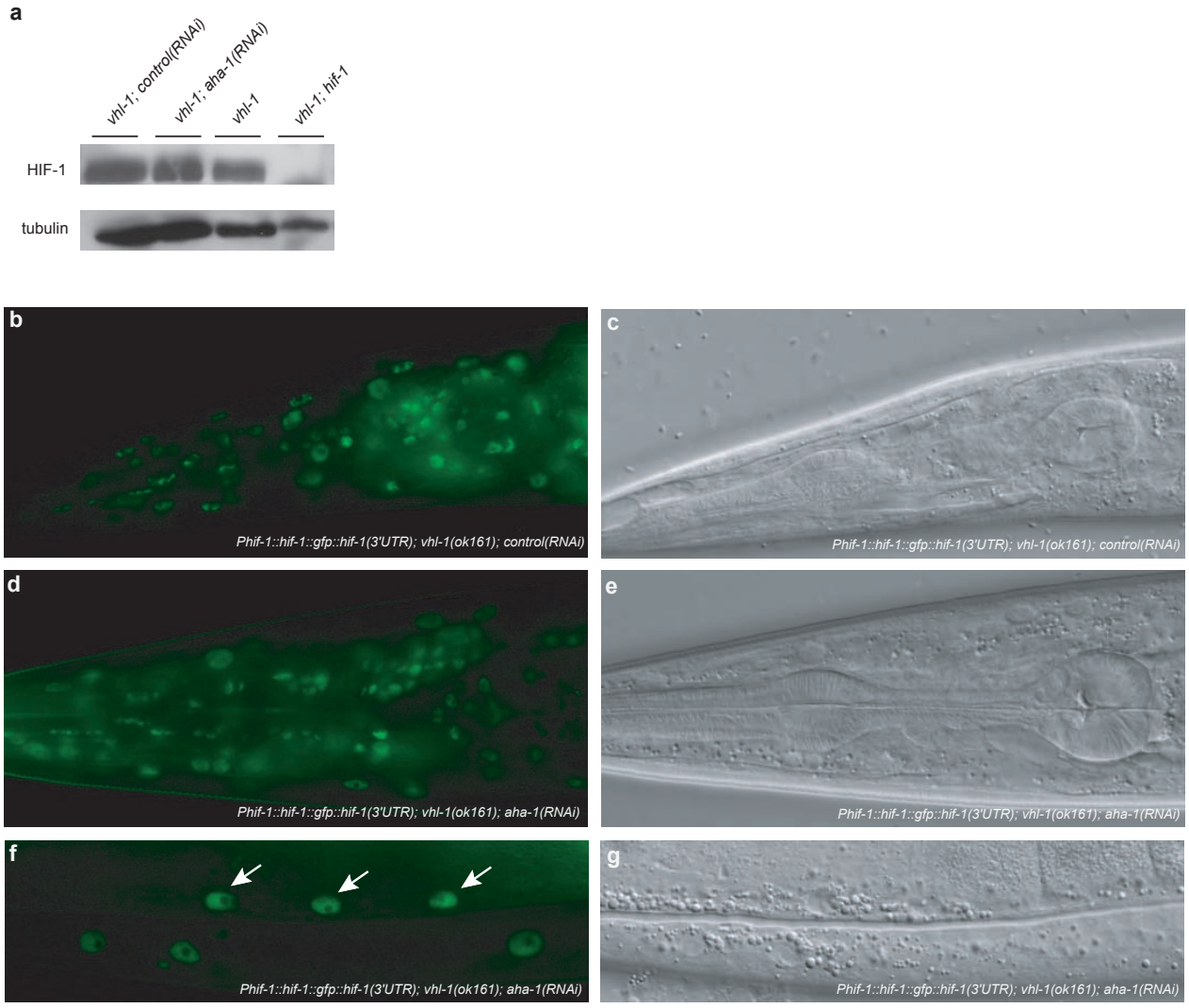

Supplementary Figure 5. HIF-1alpha is expressed and localizes to the nucleus also in the absence of HIF-1beta.
a, HIF-1beta does not influence HIF-1 alpha expression. HIF-1 western blot analysis of synchronized young adults animals.
b-g, HIF-1 localizes to the nucleus independently of HIF-1beta. Synchronized *opIs206[Phif-1::hif-1::gfp::hif-1(3'UTR)]; vhl-1(ok161)* animals were treated with either *aha-1/hif-1beta(RNAi)* or *control(RNAi)* and were analyzed for HIF-1::GFP localization. HIF-1alpha is ubiquitously detectable in the nucleus in the head region due to loss of VHL-1-dependent degradation (**b, c**).
Knock-down of HIF-1beta does not influence HIF-1alpha localization as shown in the head region (**d, e**) or in hypodermal cells (**f, g**).

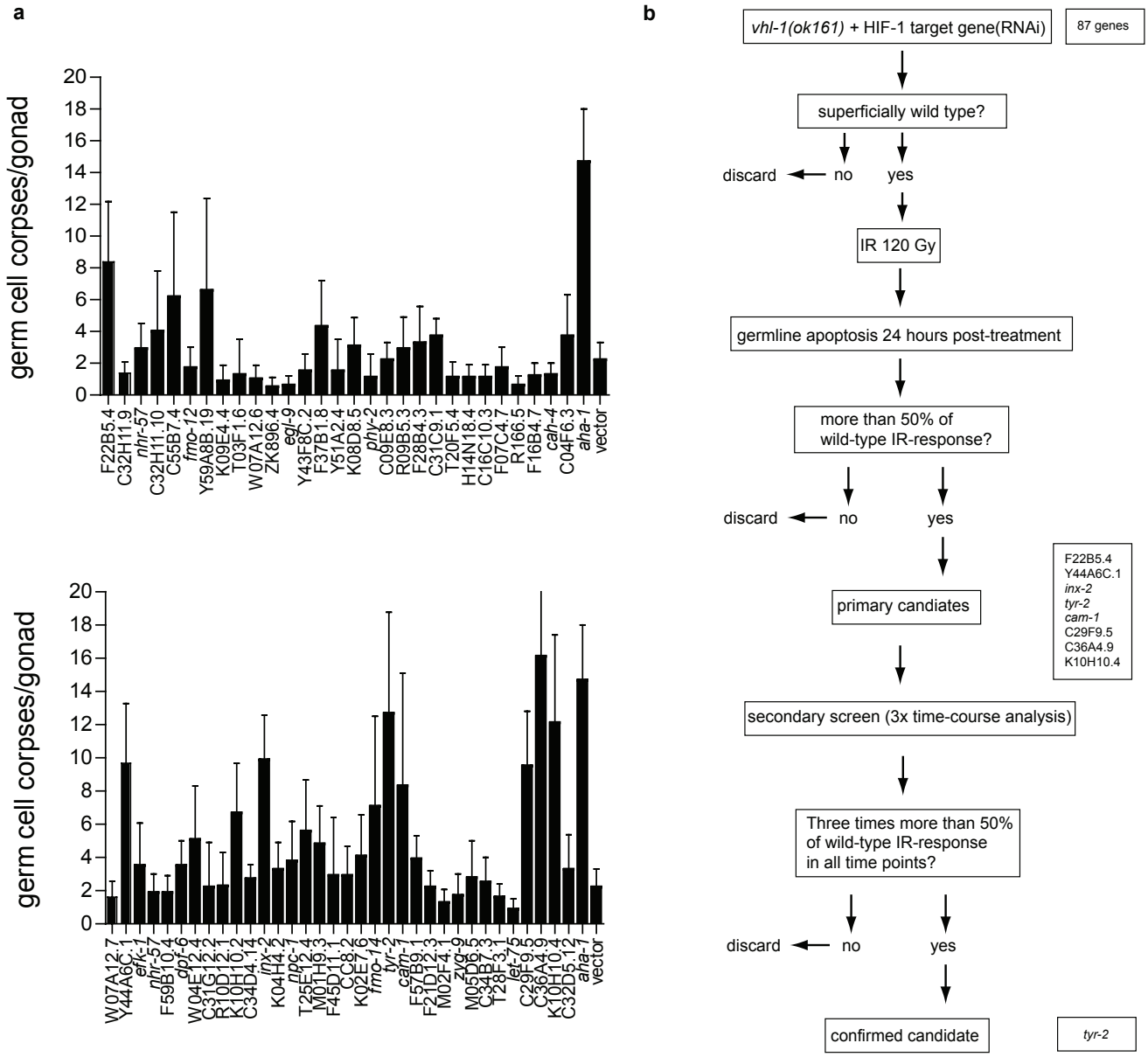

Supplementary Figure 6. A RNAi screen to identify genes that mediate resistance to DNA damage-induced apoptosis in *vhl-1(ok161)* mutants.

a, Primary screen to identify HIF-1 target genes which, when knocked-down by RNAi, restore IR-induced germline apoptosis in *vhl-1(ok161)* mutants. HIF-1 target genes identified in two previous microarray studies[16, 17] were knocked-down in *vhl-1(ok161)* mutant worms. Animals were irradiated with 120 Gy upon reaching young adult stage and germline apoptosis was quantified 24 hours post-treatment. Data shown represents the average of 20 worms ± s.d.

b, Design of the screen to identify HIF-1 target genes which restore IR-induced apoptosis in *vhl-1(ok161)* mutant animals. The primary screen identified eight candidates with an IR-response that was at least 50% of the wild-type IR-response. Out of these candidates, only *tyr-2* consistently restored (three time-course experiments) DNA damage-induced apoptosis in *vhl-1(ok161)* mutant animals.

Supplementary Figure 7 Schematic representation of the *tyr-2* (K08E3.1) locus.
a, The *ok1363* allele affects exons three, four and five, deleting 926 bp. The *tyr-2* promoter region contains three putative hypoxia-response elements (HRE) (5'-TACGTG-3'). **b,** Schematic representation of TYR-2 protein domains. TYR-2 contains a putative signal peptide (amino acids 1-22) and is composed of the tyrosinase domain (amino acids 143 to 435) and two ShKT domains (amino acids 541-577 and 585-622). **c,** Reverse transcription PCR for *tyr-2* reveals the presence of a truncated transcript in *tyr-2(ok1363)* animals, in which exon two splices in frame to exon six, deleting a large fraction of the tyrosinase domain without affecting the ShK domains.
d, Multiple alignment of the amino acid sequence of *C. elegans* TYR-2, chicken tyrosinase-related protein 2 and human tyrosinase-related protein 2. Depicted in red are six conserved histidines, which putatively bind two zinc atoms (A and B) in the catalytic center [48].

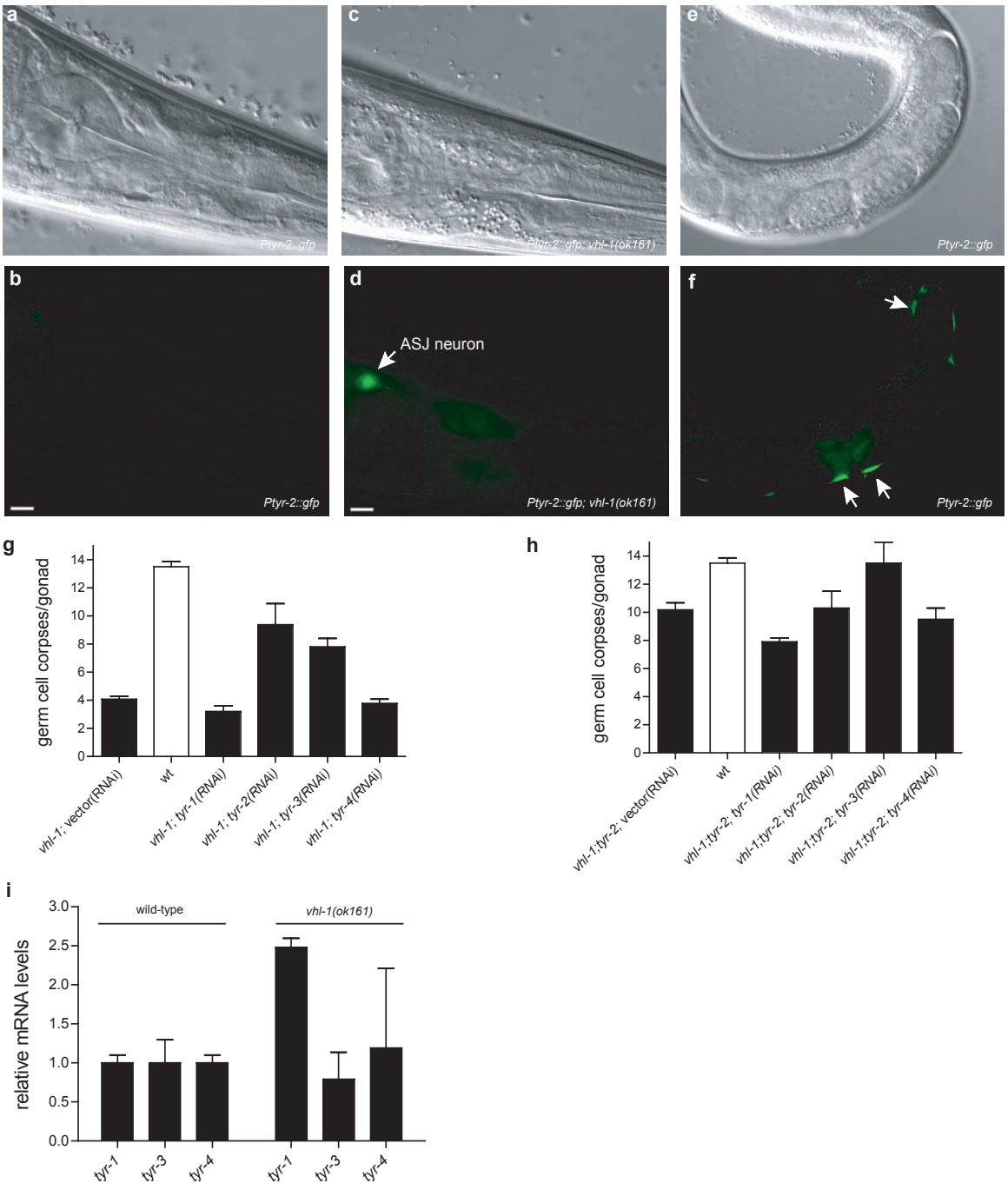

Supplementary Figure 8. HIF-1 initiates *tyr-2* transcription in the ASJ neurons.
a-d, HIF-1 stabilization by means of the *vhl-1(ok161)* mutation in the background of *opIs216[Ptyr-2::gfp]* animals results in an additional GFP signal specifically in two neurons in the head. Arrow indicates one of two ASJ sensory neurons.
e, f, GFP signal in the uterine muscles (arrows) in *opIs216[Ptyr-2::gfp]* animals which is not dependent on HIF-1 activity.
g, h, TYR-3 acts partially redundant with TYR-2. Germ cell apoptosis quantification upon IR 120 Gy in synchronized young adult animals 24 hours post-treatment. Data shown represent the average of three independent experiments ± s.d.
(n>20 animals for each experiment and time point).
i, TYR-3 transcription is not controlled by HIF-1. Synchronized young adult animals were analyzed for *tyr-1, tyr-3* and *tyr-4* mRNA levels by quantitative RT-PCR. Transcript levels were normalized to *tbp-1* and *pgk-1*. Data shown represent the average from two independent experiments in triplicates ± s.d.

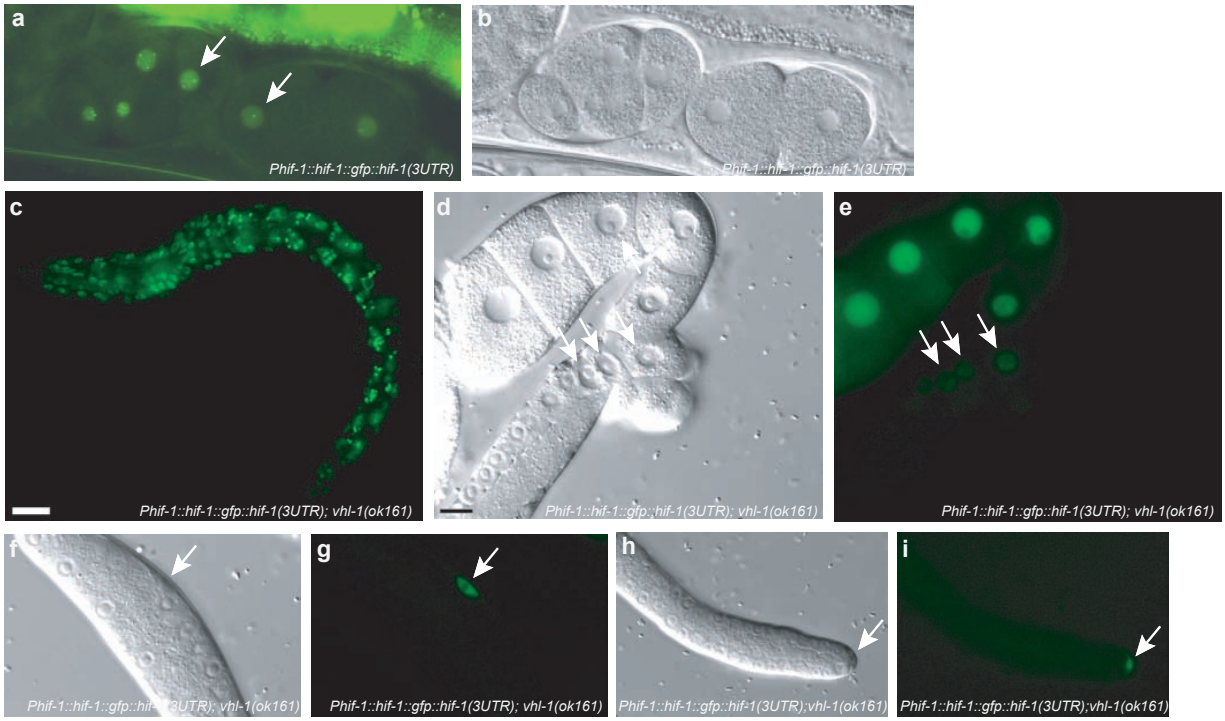

Supplementary Figure 9. HIF-1 is not detectable in the pachytene zone of the gonad.
To study HIF-1 localization, the translational GFP reporter *opIs206[Phif-1::hif-1::gfp::hif-1(3'UTR)]* was constructed. Under normoxia, HIF-1::GFP was not detectable in larvae or adults due to rapid HIF-1 degradation by the proteasome. **a, b,** In embryos, however, HIF-1::GFP was detected (arrows) even under normoxia (arrows). **c,** HIF-1 stabilization by the *vhl-1(ok161)* mutation results in accumulation of HIF-1::GFP in all somatic tissue. Scale bar, 40μm.
d, e, In the germ line of *vhl-1(ok161)* mutants, HIF-1::GFP is not observed in the mitotic and early meiotic gonad, but appears in maturing oocytes (arrows). Scale bar, 20 μm. **f, g,** Transition and pachytene germline zones in *opIs206; vhl-1(ok161)* animals. HIF-1::GFP is absent in germ cells, but present in the somatic sheath cells (arrow). **h, i,** Mitotic and transition germline zones in *opIs206; vhl-1(ok161)* animals. While HIF-1::GFP is absent in mitotic germ cells, arrows point at HIF-1 expression in the distal tip cell (DTC).

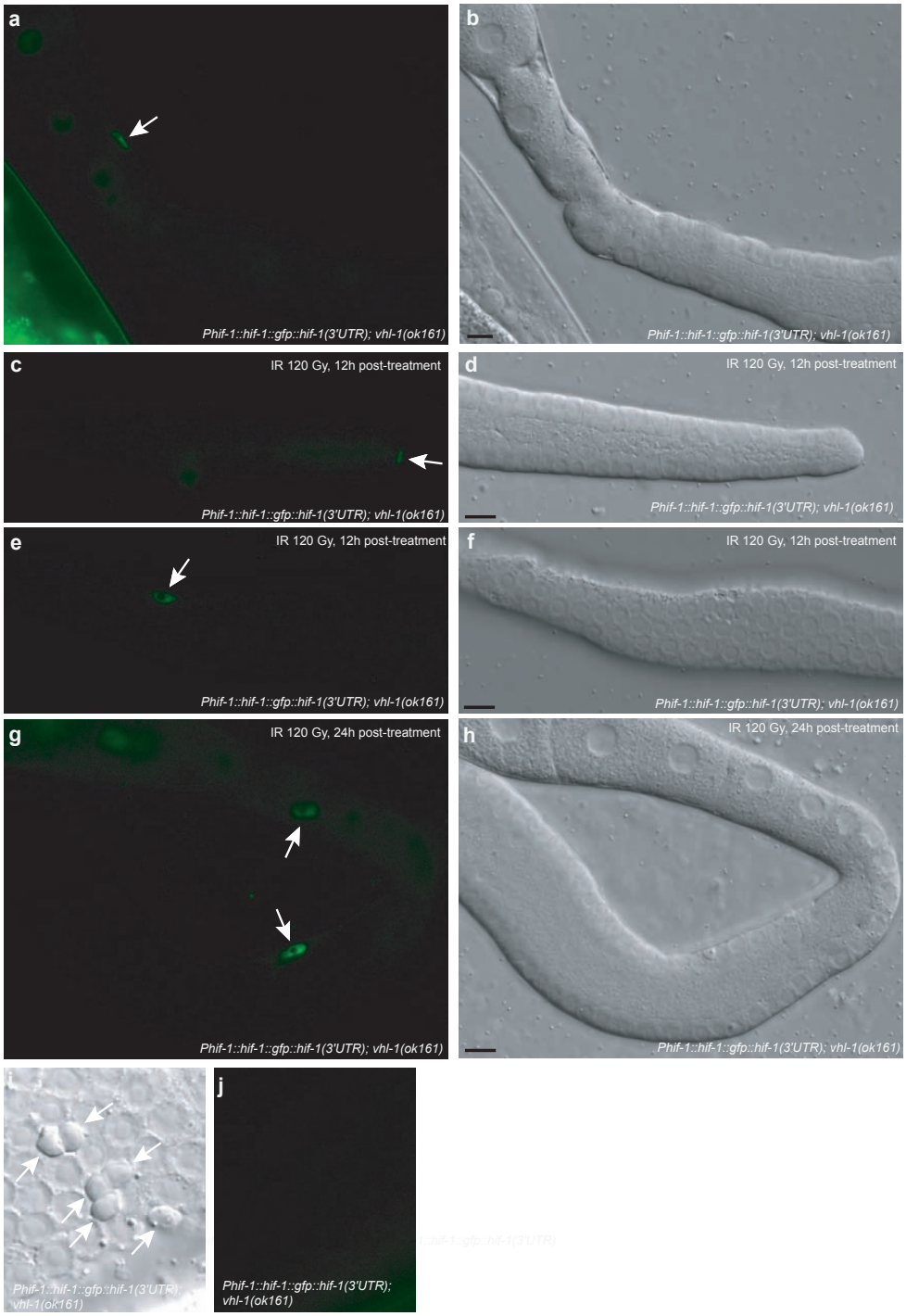

Supplementary Figure 10. HIF-1 is not detectable in the germ line of *vhl-1(ok161)* mutants following IR.
a-h,To study HIF-1 localization following ionizing radiation, *opIs206[Phif-1::hif-1::gfp::hif-1(3'UTR)]; vhl-1(ok161)* animals were irradiated, gonads were dissected and analyzed for HIF-1 appearance. Arrows point at somatic gonadal sheet cells **(a, e, g)** and at the distal tip cell **(c)**, where HIF-1 is constitutively expressed in a *vhl-1* mutant background. By contrast, no GFP staining is apparent in germ cells. Size bar, 10 μm.
i-j, HIF-1 is not detectable in cells undergoing apoptosis. Arrows indicate apoptotic cell corpses in the germ line.

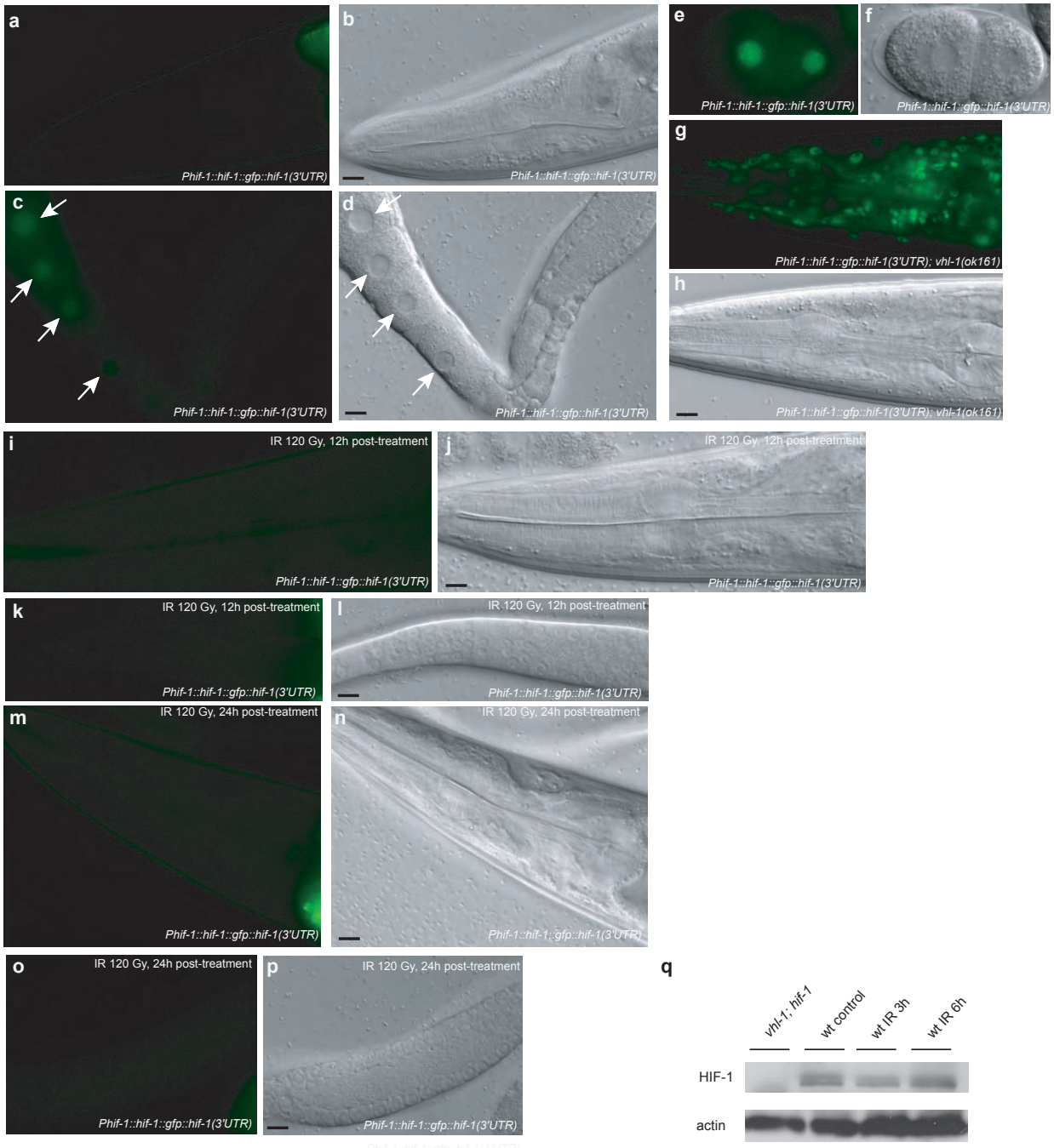

Supplementary Figure 11. Ionizing radiation does not induce HIF-1 expression in *C. elegans.*
a, b, HIF-1 is not detectable in the somatic tissue of *opIs206[Phif-1::hif-1::gfp::hif-1(3'UTR)]* animals under normoxia. However, in mature oocytes (**c, d**) and in early embroys (**e, f**), HIF-1 is regulated independently of VHL-1 and readily detectable in the nucleus even under normoxia. Arrows point at oocytes in the germ line. Size bar, 10 μm
g, h, HIF-1::GFP in the head region of animals with loss of VHL-1. Size bar, 10 μm
i-p, IR does not induce HIF-1. Synchronized young adult animals were irradiated (120 Gy) and assessed for HIF-1 expression in the head region **(i, j, m ,n)** or in the germ line (**k, l, o, p**) 12h and 24h post-treatment. Size bar, 10 μm.
q, Western blot analysis for HIF-1 does not show any increase in HIF-1 upon IR (120 Gy). Synchronized young adult animals were irradiated and HIF-1 was tracked 3h and 6h post-treatment. Since HIF-1 in oocytes and early embryos is regulated independently of VHL-1, the degree of detectable HIF-1 in wild-type worms is dependent on the amount of embryos and oocytes in the sample.

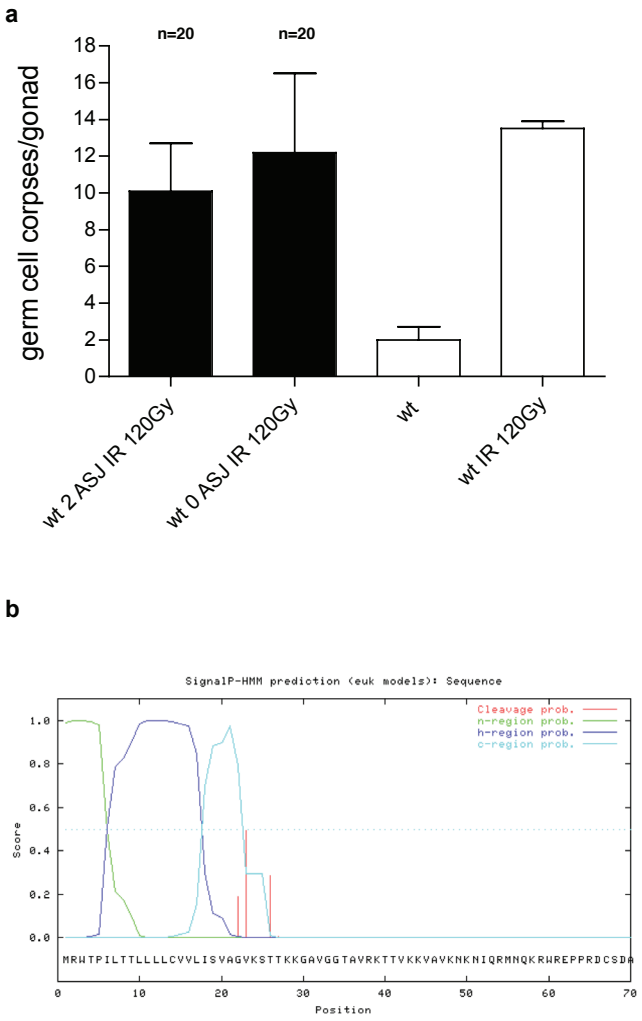

Supplementary Figure 12. Laser ablation of the ASJ neurons does not sensitize wild-type animals to IR.
a, Germ cell apoptosis quantification of ASJ-ablated wild-type animals. Synchronized L1/L2 wild-type animals were stained with DiD. ASJ sensory neurons were either ablated or mock-ablated. Worms were allowed to recover on plates and then irradiated upon reaching young adult stage. Germline apoptosis was quantified 24 hours post-treatment and the number of intact ASJ neurons was determined. Number of intact ASJ sensory neurons are indicated. Data shown represent the average of 20 animals ± s.d.
b, Analysis of the TYR-2 amino acid sequence using SignalP 3.0 reveals a putative signal peptide in the TYR-2 amino acid sequence (probability 0.989), and a maximal cleavage site probability between position 22 and 23 (probability 0.495)(ref.49).

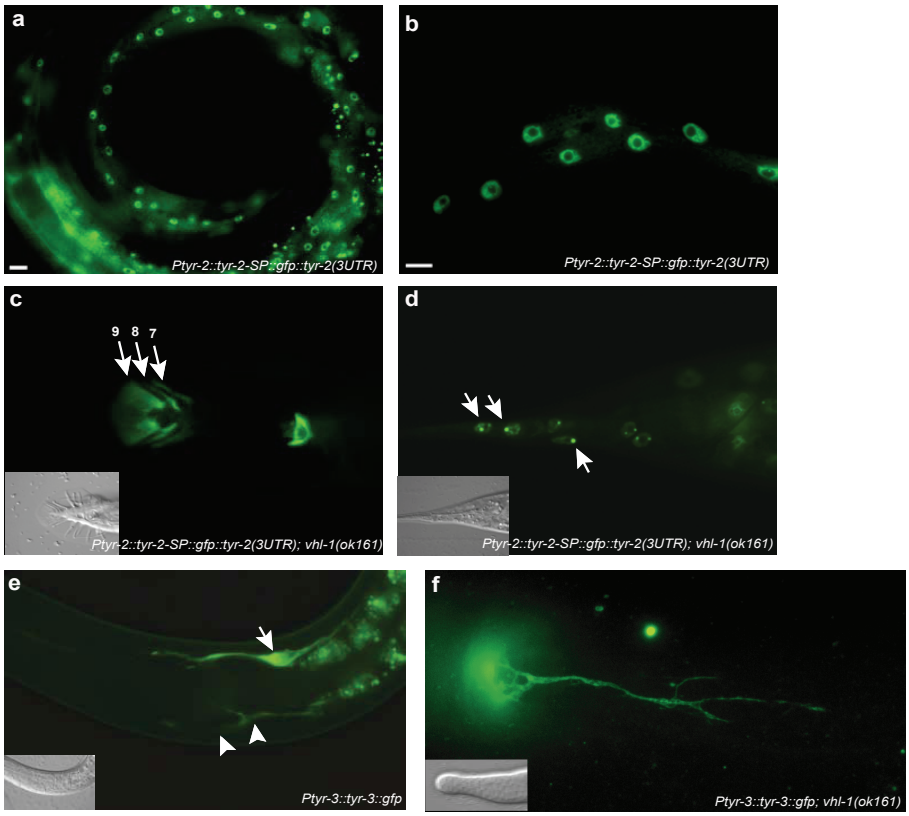

Supplementary Figure 13. Expression pattern of TYR-2 lacking the signal peptide and of TYR-3.
a, TYR-2::GFP reporter lacking the signal peptide (SP) (amino acids 1-22) shows nuclear expression in the hypodermis and uterine muscles. Scale bar, 10μm. **b,** Higher magnification of hypodermal expression of TYR-2 GFP reporter lacking the signal peptide. Scale bar, 10μm. **c,** TYR-2-SP::GFP in the male tail shows expression in rays 7, 8 and 9 (arrows). **d,** TYR-2-SP::GFP expression the hermaphrodite tail region. Note the bright foci (arrows) around the nucleolus, usually two per nucleus.
e, *opIs271[Ptyr-3::tyr-3::gfp::tyr-3(3'UTR)]* animals show TYR-3 expression in the head mesodermal cell (hmc) (arrow). Arrowheads indicate ventral processes of the hmc. **f,** TYR-3 distal tip cell expression in *opIs271[Ptyr-3::tyr-3::gfp::tyr-3(3'UTR)]; vhl-1(ok161)* animals.

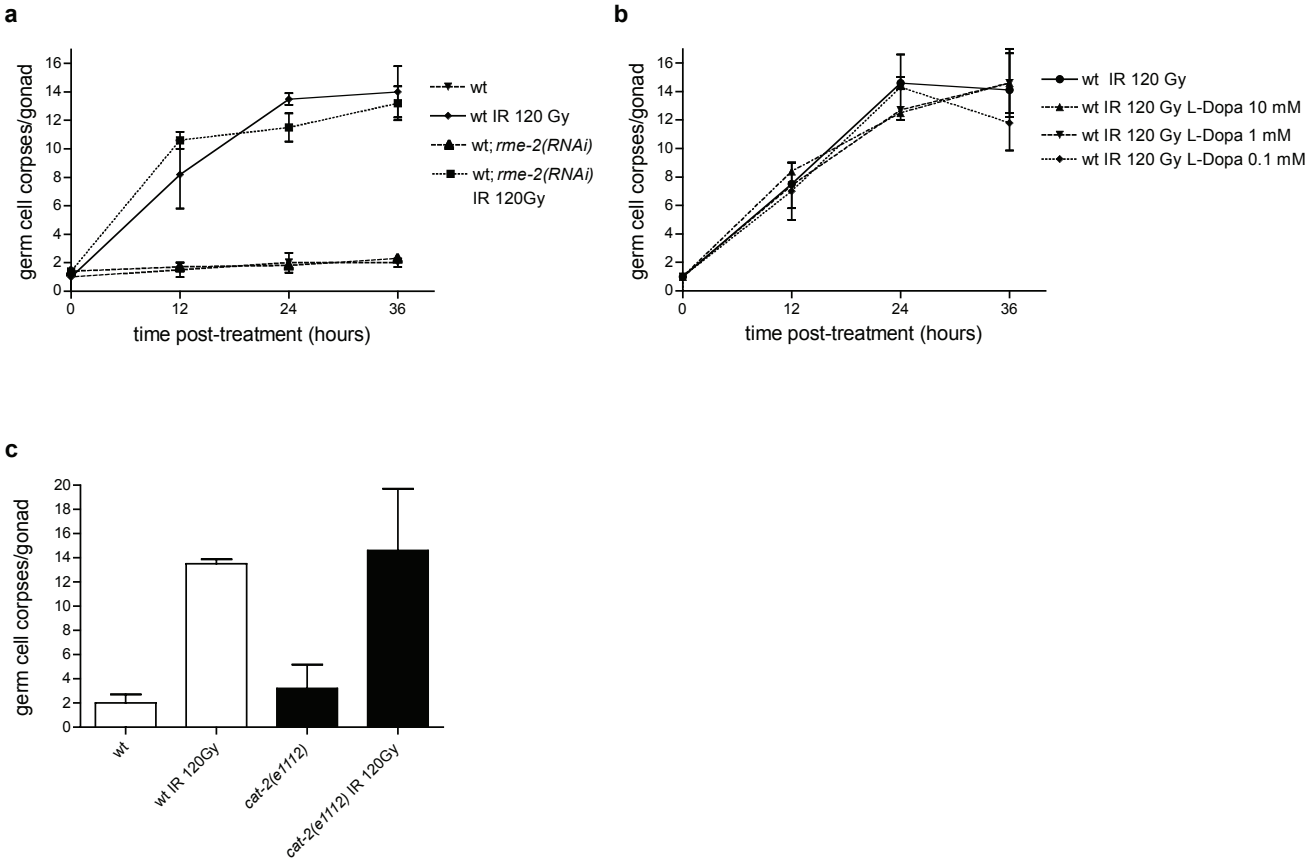

Supplementary Figure 14. Analysis of the alternative possibilty that small diffusible molecules could antagonize DNA damage-induced apoptosis.

a, *rme-2(RNAi)* does not alter apoptotic response in wild-type animals. Germline apoptosis time-course of wild-type worms either fed on *rme-2(RNAi)* or control(RNAi). Data shown represent the average of three independent experiments ± s.d. (n>20 animals for each experiment and time point). **b,** L-Dopa treatment does not alter DNA damage-induced germ cell apoptosis. Synchronized L3 wild-type larvae were treated with the indicated L-Dopa concentrations on plates and were then irradiated upon reaching young adult stage. Germline apoptosis was quantified at the indicated time points. Data shown represent the average of six independent experiments ± s.d. (n>20 animals for each experiment and time point).

c, The dopamine biosynthesis tyrosine hydroxylase CAT-2 does not control DNA damage-induced germ cell apoptosis. Tyrosinases could under certain circumstances function as tyrosine hydroxylases[50]. Therefore, dopaminergic influence on apoptosis was analyzed by assessing germline apoptosis in *cat-2(e1112)* mutants. Germline apoptosis quantification of control and irradiated *cat-2(e1112)* mutants 24 hours post-treatment showed no difference in the apoptotic rate. Data shown represent the average of 30 animals ± s.d.

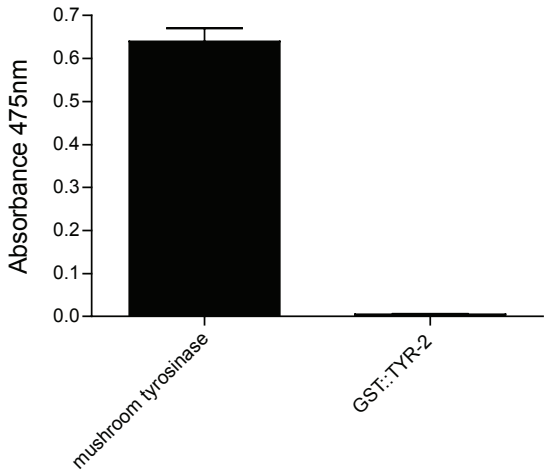

Supplementary Figure 15. GST::TYR-2 has no tyrosinase activity.
0.5 mM L-tyrosine in 0.05 M sodium phosphate buffer, pH6.8, was incubated with either mushroom tyrosinase (50 μg/ml) or GST::TYR-2 (100 μg/ml) at 25°C for 10 minutes. Absorbance was measured at 475 nm.

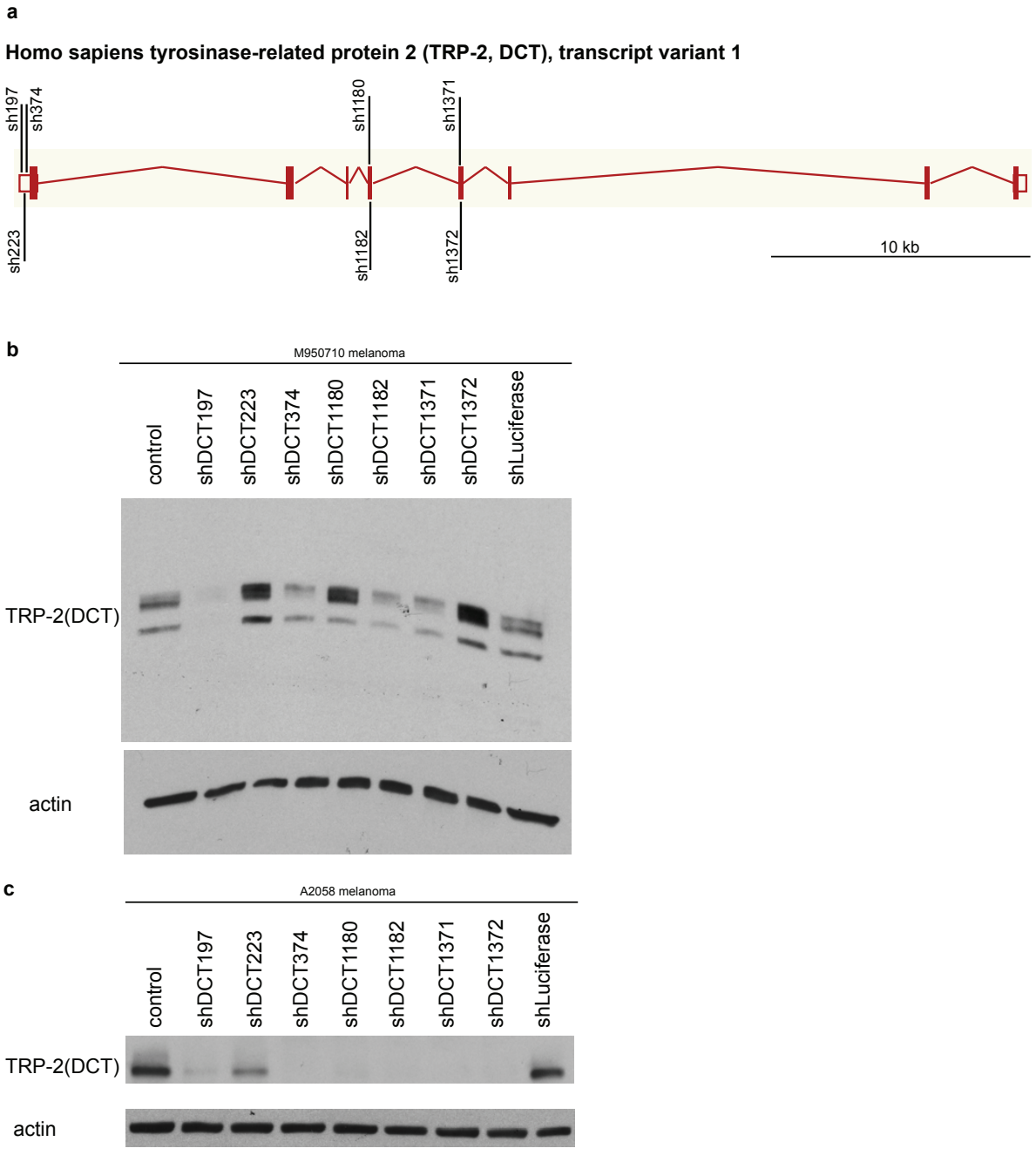

Supplementary Figure 16. Efficiency of different short hairpin RNAs against human tyrosinase-related protein 2 (TRP-2, DCT) in melanoma cells.
a, Schematic representation of the position within the *trp-2* locus of different shRNAs tested against human TRP-2(DCT). Open boxes represent 5' and 3' UTRs. Numbers represent the first nucleotide of the shRNA, the sequences can be found in the Supplementary Material and Methods.
b, c, Knock-down efficiency by different shRNAs was tested by western blot analysis using an anti-TRP-2 (Pep8) antibody (generous gift from Dr. V. Hearing) in two different melanoma cell lines.

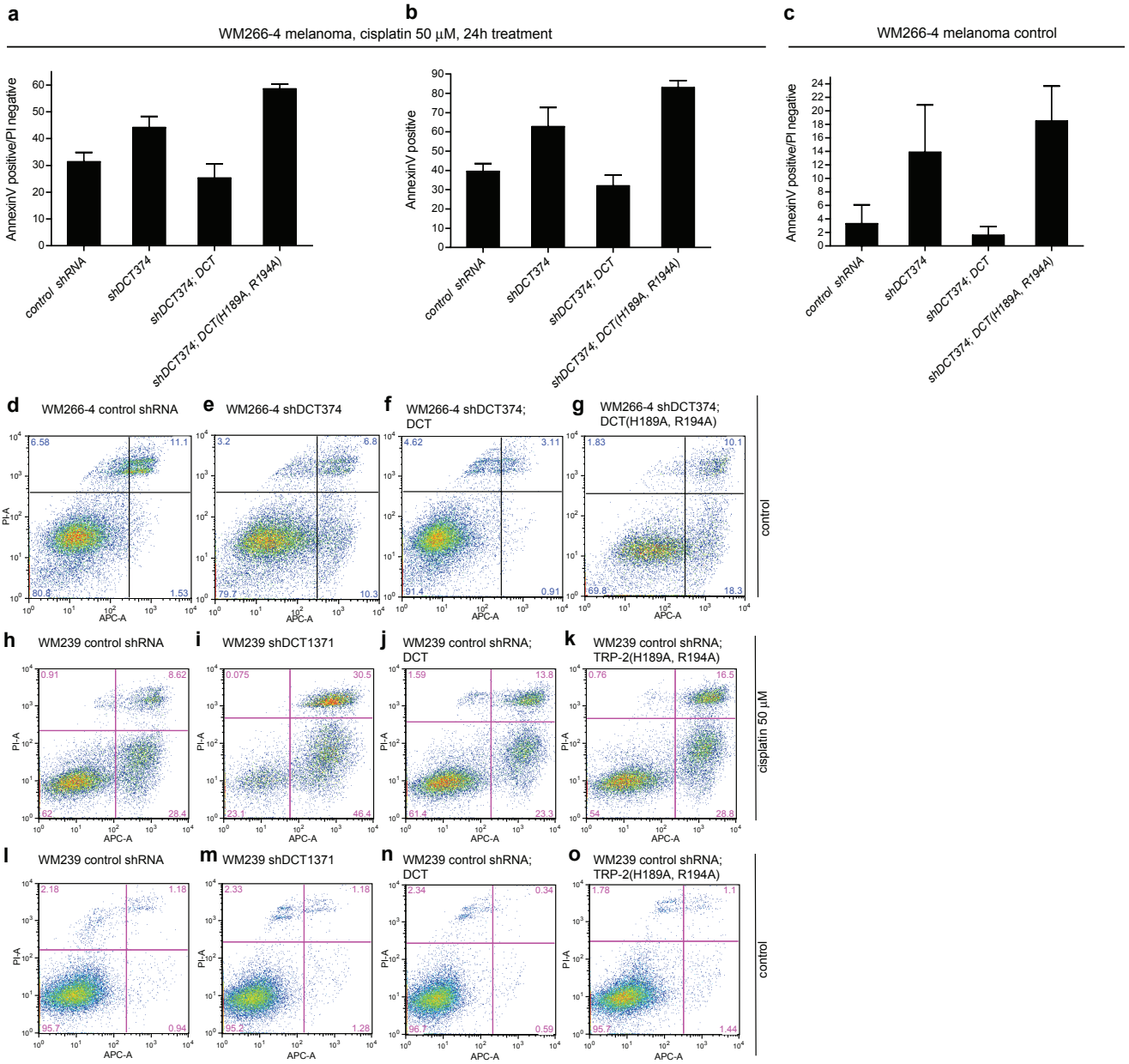

Supplementary Figure 17. Loss of human tyrosinase-related protein 2 (TRP-2, DCT) results in increased cisplatin-induced apoptosis.

a-c, Human tyrosinase-related protein 2 (TRP-2, DCT) counteracts cisplatin-induced apoptosis in WM266-4 metastatic melanoma cells. Melanoma cells were treated with 50 μM cisplatin, stained with Annexin-V-APC /PI 24h post-treatment and analyzed by flow cytometry. TRP-2 knock-down increased Annexin-V positive/PI negative fractions (early apoptotic cells) or Annexin-V positive fraction (early and late apoptotic cells) compared to control shRNA (Luciferase) knock-down in WM266-4 melanoma cells. Data represent average of four independent experiments ± s.d.

d-g, Loss of human tyrosinase-related protein 2 (TRP-2, DCT) results in increased apoptosis of untreated WM266-4 cells. Untreated WM 266-4 melanoma cells were stained with Annexin-V-APC/PI and analyzed by flow cytometry. The shDCT374 (targeting endogenous TRP-2 5'UTR) phenotype was rescued by expression of wild-type TRP-2 (MSCV-DCT) but not of catalytically inactive point mutant TRP-2(H189A, R194A) (MSCV-DCT). TRP-2(H189A, R194A); shDCT374 cells (**g**) showed even higher apoptotic levels than shDCT374 cells (**e**) suggesting a dominant negative effect of the point-mutated TRP-2 version.

h-o, Loss of human TRP-2 results in increased cisplatin-induced apoptosis also in WM239 melanoma cells .
Melanoma cells were treated with 50 μM cisplatin, stained with Annexin-V-APC/PI 24h post-treatment and analyzed by flow cytometry. TRP-2 knock-down increased Annexin-V positive/PI negative fractions (early apoptotic cells) compared to control shRNA (shLuciferase) knock-down.

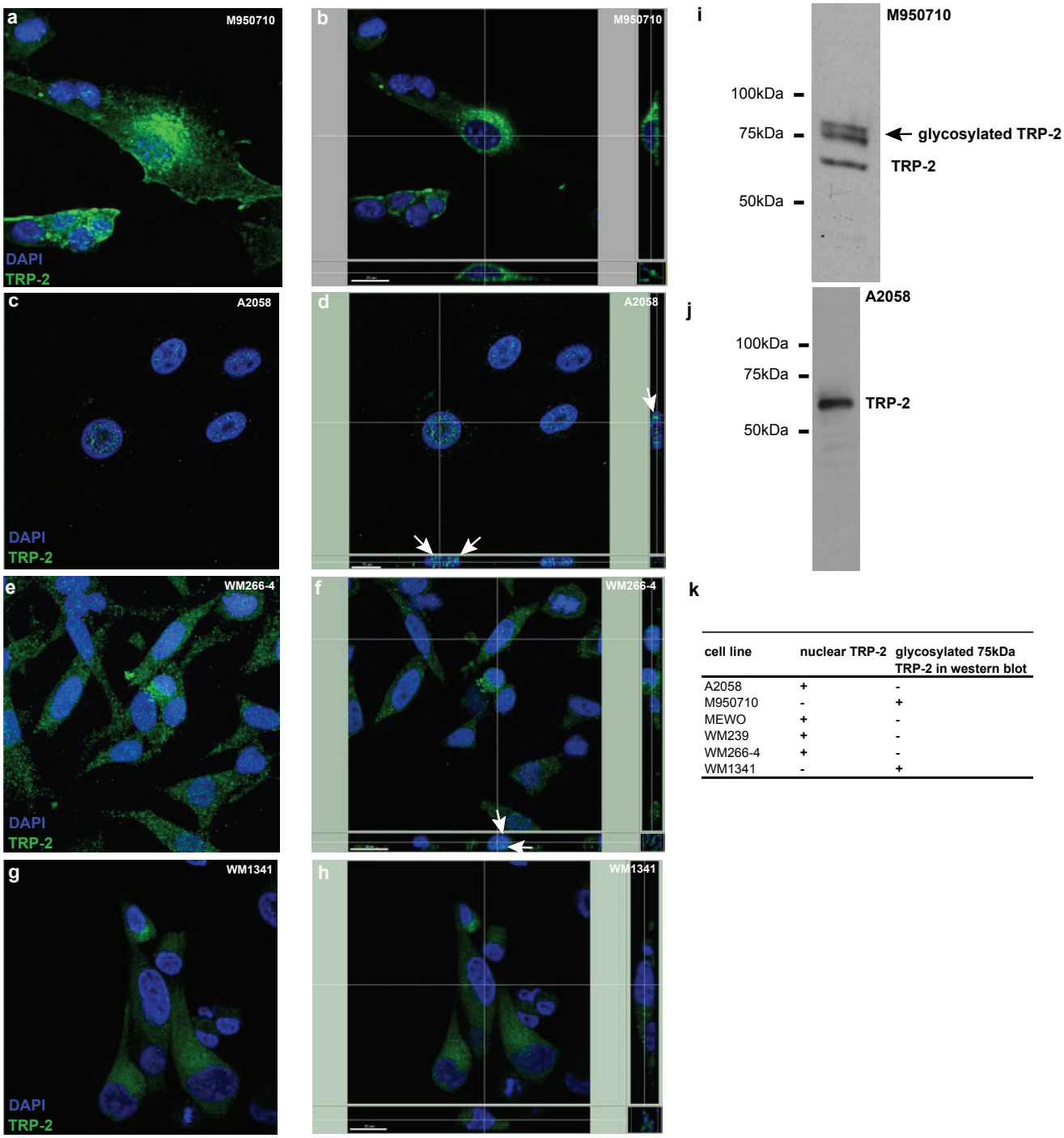

k

cell line	nuclear TRP-2	glycosylated 75kDa TRP-2 in western blot
A2058	+	-
M950710	-	+
MEWO	+	-
WM239	+	-
WM266-4	+	-
WM1341	-	+

Supplementary Figure 18. TRP-2 localizes to the nucleus in some melanoma cell lines.
a-h, M950710, A2058, WM266-4 and WM1341 melanoma cell lines were immunostained with TRP-2 anti-Pep8 antibody (kindly provided by Dr. Vincent Hearing) and DAPI. In M950710 and WM1341 melanoma cell lines, TRP-2 is mainly detectable in the secretory pathway and is clearly excluded from to the nucleus (sections (Imaris), **b, h**).
In contrast, TRP-2 is observed in the nucleus in A2058 and WM266-4 melanoma cell lines (arrows in sections **d, f**).
i-k, Appearance of nuclear TRP-2 correlates with a TRP-2 band that migrates differently in western blot analysis, suggesting that nuclear TRP-2 might represent a differently processed version of the protein.

a CEP-1/p53 sequence coverage:

MEPDDSQLSDILKDARIPDSQDIGVNLTQNLSFDTVQKMIDGVFTPIFSQ
GTEDSLEKDILKTPGISTIYNGILGNGEETKKRTPKISDAFEPDLNTSGD
VFDSDKSEDGLMNDESYLSNTTLSQVVLDSQKYEYLRVRTEEEQQLVIEK
RARERFIRKSMKIAEETALSYENDGSRELSETMTQKVTQMDFTETNVPFD
GNDESSNLAVRVQSDMNLNEDCEKWMEIDVLKQKVAKSSDMAFAISSEHE
KYLWTKMGCLVPIQVKWKLDKRHFNSNLSLRIRFVKYDKKENVEYAIRNP
RSDVMKCRSHTEREQHFPFDSFFYIRNSEHEFSYSAEKGSTFTLIMYPGA
VQANFDIIFMCQEKCLDLDDRRKTMCLAVFLDDENGNEILHAYIKQVRIV
AYPRRDWKNFCEREDAKQKDFRFPELPAYKKASLESINIKQEVNLENMFN
VTNTTAQMEPSTSYSSPSNSNNRKRFLNECDSPNNDYTMMHRTPPVTGYA
SRLHGCVPPIETEHENCQSPSMKRSRCTNYSFRTLTLSTAEYTKVVEFLA
REAKVPRYTWVPTQVVSHILPTEGLERFLTAIKAGHDSVLFNANGIYTMG
DMIREFEKHNDIFERIGIDSSKLSKYYEAFLSFYRIQEAMKLPK

b

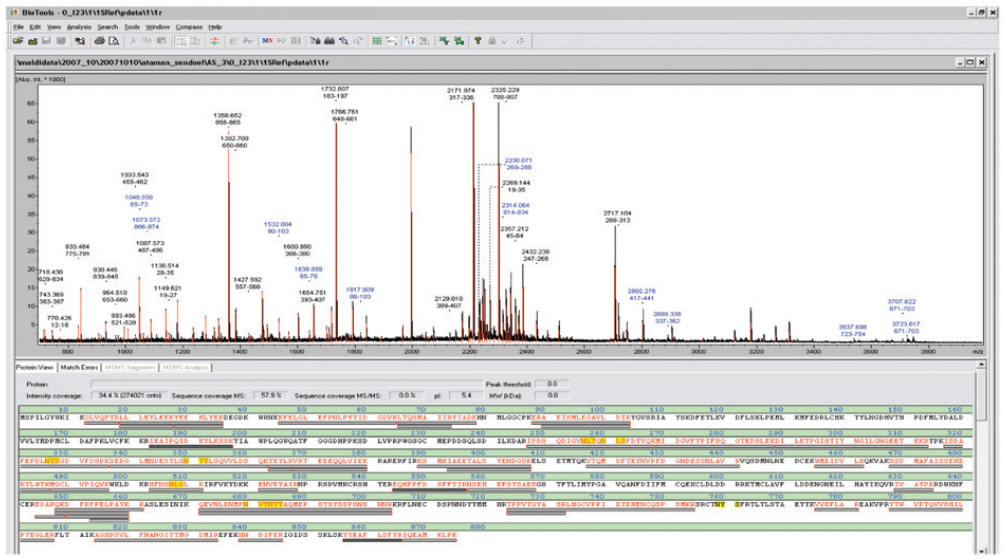

c

Supplementary Figure 19. GST::CEP-1 MS/MS analysis.
a, CEP-1 sequence coverage from three independent experiments is shown in gray. Representative panel, where GST::CEP-1 was incubated either **b,** alone or with **c,** GST::TYR-2 for two hours in 0.05 M phosphate buffer, pH 6.8, 25°C. The proteins were analyzed on a SDS-PAGE gel and GST::CEP-1 was analyzed by MALDI-MS and MALDI-MS-MS.

a CEP-1/p53 peptide: SFFYIRNSEHEFSYSAEK
Theoretical mass: 2241

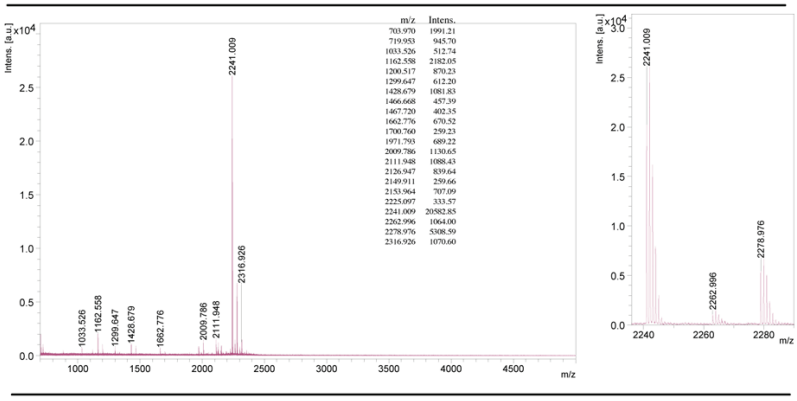

b

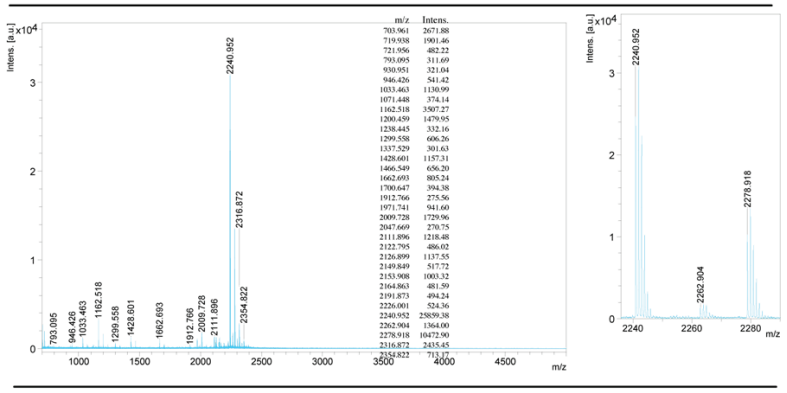

Supplementary Figure 20. GST::TYR-2 does not result in a mass shift of the synthetic CEP-1/p53 model peptide. The synthetic CEP-1/p53 peptide SFFYIRNSEHEFSYSAEK (synthesized by Sigma) was chosen as a model peptide and incubated either **a,** alone or with **b,** GST::TYR-2 for two hours in 0.05 M phosphate buffer, pH 6.8, 25°C. The mass of the peptide in solution was directly analyzed by MALDI-MS.

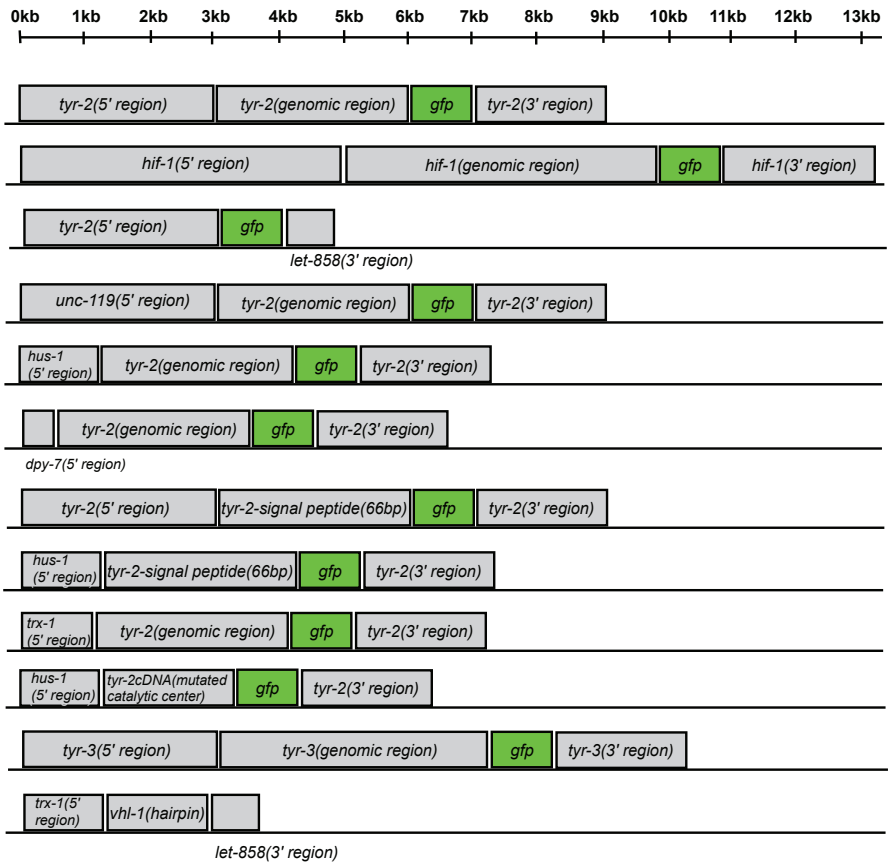

Description	Transgenic lines
endogenous promoter, full genomic region	*opIs407, opIs240*
endogenous promoter, full genomic region	*opIs206*
transcriptional *tyr-2* reporter	*opIs216, opIs217*
panneuronal promoter	*opIs233, opIs234*
germline promoter	*opIs245*
hypodermal promoter	*opIs241*
endogenous promoter, signal peptide (22aa) deleted from the *tyr-2* genomic region	*opEx1321,opEx1322, opEx1323*
germline promoter, signal peptide (22aa) deleted from the *tyr-2* genomic region	*opEx1344,opEx1345, opEx1346, opEx1347, opEx1348,opEx1350, opEx1351*
ASJ promoter	*opIs316*
germline promoter, signal peptide deleted H195A, H205A, H214A, H336A, H340A, H363A	no expressing line obtained
endogenous promoter, full genomic region	*opIs271*
tissue-specific hairpin RNAi ASJ-spedific promoter	*opIs425*

Supplementary Figure 21.
Schematic representation of the constructs used to generate transgenic lines in this study.

Supplementary Table 1 l HIF-1 does not influence DNA repair

	0 Gy	30 Gy	60 Gy	120 Gy
genotype	**survival [%]**	**survival [%]**	**survival [%]**	**survival [%]**
wild-type	98.9 ± 0.1	95.1 ± 4	92.5 ± 4	72.4 ± 15
vhl-1(ok161)	98.6 ± 0.4	92.1 ± 5	93.1 ± 6	78.8 ± 16
hif-1(ia4)	97.5 ± 0.1	94.4 ± 3	91.7 ± 8	81.8 ± 8
rad-5(mn159)	92.4 ± 5	51.5 ± 3	8.3 ± 2	0.7 ± 1

Embryonic lethality of synchronized animals following 0 Gy, 30 Gy, 60 Gy, 120 Gy IR. Synchronized L4 animals were irradiated. Animals were allowed to lay eggs for 8 hours, 24 hours post-treatment. Number represent average survival percentage from three to four independent experiments ± s.d.

Supplementary Table 2 l TYR-2 antagonizes apoptosis cell non-autonomously

		control		IR	
genotype	Promoter	24h	36h	24h	36h
wild type	-	1.8±0.7	1.8±0.3	13.5±0.4	14.0±1.8
vhl-1(ok161)	-	0.7±0.5	1.5±0.2	1.0±0.2	1.6±0.3
tyr-2(ok1363)	-	4.2±1.1	9.5±0.9	16.7±0.7	16.5±3.3
Punc-119::tyr-2::gfp::tyr-2(3U'TR); tyr-2(ok1363)	panneuronal	1.7±0.2	2.6±1.1	3.3±0.6	5.4±1.3
Pdpy-7::tyr-2::gfp::tyr-2(3'UTR); tyr-2(ok1363)	hypodermal	1.3±0.1	2.4±0.4	5.1±2.8	4.9±2.3
Phus-1::tyr-2::gfp::tyr-2(3'UTR); tyr-2(ok1363)	germ line	1.5±0.3	1.7±0.3	3.6±1.6	4.7±1.9
Ptrx-1::vhl-1(hairpin)::let-858(3'UTR)	ASJ neuron	3.0±0.8	2.9±0.2	4.5±0.2	5.8±1.0

Quantification of germline apoptosis in synchronized young adult transgenic animals following IR 120 Gy. Data shown represents the average of two to four independent experiments ± s.d. (n>20 animals for each experiment and time-point).

Supplementary References

47. Stergiou, L. & Hengartner, M. O. Death and more: DNA damage response pathways in the nematode *C. elegans. Cell Death Differ* **11**, 21-8 (2004).

48. Solano, F., Martinez-Liarte, J. H., Jiménez-Cervantes, C., García-Borrón, J. C. & Lozano, J. A. Dopachrome tautomerase is a zinc-containing enzyme. *Biochem Biophys Res Commun* **204**, 1243-50 (1994).

49. Bendtsen, J. D., Nielsen, H., von Heijne, G. & Brunak, S. Improved prediction of signal peptides: SignalP 3.0. *J Mol Biol* **340**, 783-95 (2004).

50. Rios, M. *et al*. Catecholamine synthesis is mediated by tyrosinase in the absence of tyrosine hydroxylase. *J Neurosci* **19,** 3519-26 (1999).